Optics Letters

Selective propagation and beam splitting of surface plasmons on metallic nanodisk chains

Yuhui Hu,[1] Di Zhao,[1] Zhenghan Wang,[1] Fei Chen,[1] Xiang Xiong,[1] Ruwen Peng,[1,2] and Mu Wang[1,3]

[1]National Laboratory of Solid State Microstructures, School of Physics, and Collaborative Innovation Center of Advanced Microstructures, Nanjing University, Nanjing 210093, China
[2]e-mail: rwpeng@nju.edu.cn
[3]e-mail: muwang@nju.edu.cn

Received 13 March 2017; accepted 20 March 2017; posted 3 April 2017 (Doc. ID 290558); published 24 April 2017

Manipulating the propagation of surface plasmons (SPs) on a nanoscale is a fundamental issue of nanophotonics. By using focused electron beam, SPs can be excited with high spatial accuracy. Here we report on the propagation of SPs on a chain of gold nanodisks with cathodoluminescence (CL) spectroscopy. Experimental evidence for the propagation of SPs excited by the focused electron beam is demonstrated. The wavelength of the transmitted SPs depends on the geometrical parameters of the nanodisk chain. Furthermore, we design and fabricate a beam splitter, which selectively transmits SPs of certain wavelengths to a specific direction. By scanning the sample surface point by point and collecting the CL spectra, we obtain the spectral mapping and identify that the chain of the smaller nanodisks can efficiently transport SPs at shorter wavelengths. This Letter provides a unique approach to manipulate in-plane propagation of SPs.

OCIS codes: (240.6680) Surface plasmons; (260.2110) Electromagnetic optics; (070.4790) Spectrum analysis; (050.6624) Subwavelength structures.

https://doi.org/10.1364/OL.42.001744

Surface plasmons (SPs) [1,2] are the collective oscillation of free electrons at a metal-dielectric interface, which can efficiently confine electromagnetic fields in a limited space and be applied in subwavelength photonic devices [3–12]. It has been suggested that a queue of separated metallic nanodisks has the potential to transport information and electromagnetic energy with the advantage of selective propagation of alternating electric signals, while keeping the insulation to a direct electric signal [13,14]. This feature relies on near-field coupling of SP resonance on adjacent disks [15]. Measuring the optical spectra is an effective way to analyze radiation of SPs along the chain and the coupling of neighboring parts in energy transmission [16–19].

Traditionally, SPs on a metallic nanodisk chain are excited by a plane wave, and they are normally treated as the resonance of coupled dipoles [20–24]. However, with incidence of a polarized plane wave, the distributions of surface charge density of the modes excited by plane waves are anti-symmetrical along the polarization direction and symmetrical in the direction perpendicular to the polarization. Hence, some modes that are symmetrical along the polarization direction cannot be excited with the planar wave [25–29]. Instead of using planar electromagnetic waves, people can excite SP by a focused electron beam, with the unique advantages of richer excitation modes and much higher spatial resolution. Moreover, by exciting the sample point by point and collecting corresponding luminescence spectra, a spatial distribution of the luminescence capability over the structure can be identified [30,31]. Those spots with maximum intensity on the mapping suggest that by focusing an electron beam on these specific sites, a SP (hence, luminescence) can be most efficiently excited on the structure.

In this Letter, with cathodoluminescence (CL) spectroscopy, we investigate the propagation of SPs on a chain of gold nanodisks. By introducing different substrates at specific parts of the chain and identifying the distinctive resonant peaks, we provide direct experimental evidence of the propagation of SPs excited by the focused electron beam. Further, we design a beam splitter for SPs, which selectively transmits SPs with certain wavelengths to the specific direction. By collecting CL emission mapping of the nanodisk chains with different geometrical parameters, we find that the chain with smaller nanodisks is more efficient in transporting high-frequency SPs, which corresponds to a dipolar resonance on the gold disk; the chains with larger nanodisks are more efficient to transport lower-frequency SPs, which corresponds to a quadrupole resonant mode on the disk. We suggest that this investigation is helpful in designing SP-related optical devices.

A chain of gold nanodisks is fabricated on the silicon substrate by lift-off technology. The gold layer is 60 nm in thickness. For stronger adhesion, a layer of 2 nm thick titanium is homogeneously deposited on the silicon surface before gold deposition.

In order to verify that SPs are excited by the electron beam and transport along the chain of gold nanodisks, we fabricate a nanodisk chain on a hybrid substrate surface: part of the substrate is covered with a layer SiO_2 (20 nm in thickness), and the rest of the surface remains silicon only. The chain of gold nanodisks lies across the boundary of SiO_2/Si, as shown in Fig. 1(a).

The lift-off fabricated sample is demonstrated in Fig. 1(b), where the diameter of the nanodisks is 120 nm, with a gap of 10 nm in between. Energy-dispersive x-ray spectroscopy (Inca X-MAX, Oxford Instruments) is applied to analyze the chemical element distribution on the sample surface [Fig. 1(c)]. Figure 1(c) indicates that the nanodisk chain sits on SiO_2 on the left side, and stays on the Si surface on the right side. Then we focus an electron beam at the very right end, which is the farthest from the SiO_2/Si boundary, and collect a CL spectrum over the whole sample. If the intrinsic peak of SiO_2 can be identified in the spectrum, it suggests that the SP excited by the electron beam propagates along the chain and eventually excites the luminescence of SiO_2 on the other end.

In CL (Gatan Mono CL4) experiments, a 10 keV electron beam is focused on a gold nanodisk chain as a local excitation source [Fig. 2(a)], and the luminescence emitted from the chain due to the SP resonance is collected by a parabolic mirror and directed to a grating spectrometer associated with a CCD camera. At each excitation site, we collect a spectrum in a wavelength range of 300–900 nm, and the integration time is set as 4.0 s. To get the CL spectral mapping images, the electron beam scans the whole sample site by site and, for each excitation site, a spectrum is collected. It follows that for each wavelength, each pixel of the mapping area possesses a luminescence intensity based on the collected spectra. The intensity distribution on this CL mapping reflects the capability of local luminescence emission induced by the electron beam.

We focus an electron beam at different excitation sites on the chain and collect the CL spectra, as illustrated in Fig. 2(b). First, we focus the electron beam on the SiO_2 part of substrate and collect a spectrum (the red curve). We find that SiO_2 has an intrinsic peak at 425 nm.

The black curve is collected by focusing the electron beam on the silicon part of the substrate, which is more than 600 nm away from the boundary of Si/SiO_2. The nearly flat spectrum indicates that the silicon substrate does not transmit SPs. We then focus the electron beam on a gold nanodisk on silicon substrate about 600 nm away from the SiO_2/Si boundary and collect the CL spectrum [blue curve in Fig. 2(b)]. For comparison, we collect the spectrum on a control sample, where the gold nanodisks stay on pure silicon substrate without any SiO_2 deposition [green curve in Fig. 2(b)]. One may find that the intrinsic peak of SiO_2 (425 nm) appears on the blue curve, which is obtained when the electron beam is not focused directly on the SiO_2 part. It is known that for air-gold-silicon/silicon oxide configuration, once a SP is excited, it propagates on both the top (gold-air) and bottom (gold-silicon/silicon oxide) interface [25]. Therefore, the straightforward interpretation of Fig. 2(b) is that the SP excited on the gold nanodisk chain propagates from the excitation site along the chain, and induces the luminescence of SiO_2. This observation is a direct evidence of the propagation of a SP along a nanodisk chain on a solid substrate.

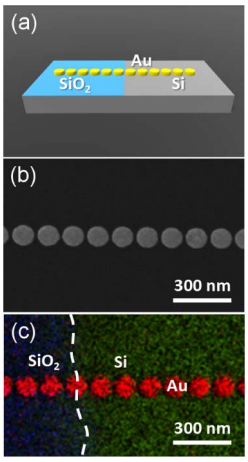

Fig. 1. (a) Schematics of a chain of Au nanodisk across the boundary of SiO_2/Si. (b) SEM micrograph of the sample. (c) Element mapping of Si (green), Au (red), and O (blue) across the boundary area.

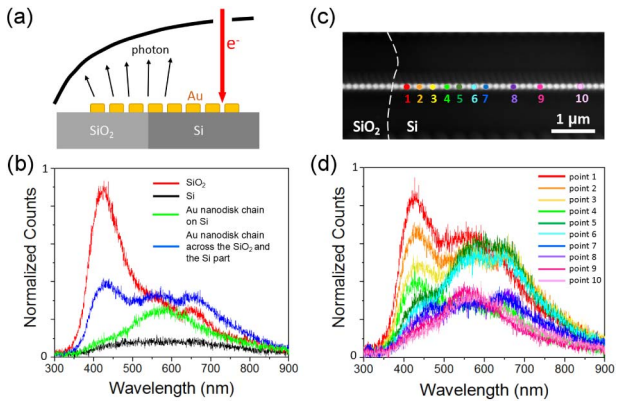

Fig. 2. (a) Sketch of a CL system. An electron beam incidents a normal to gold nanodisk chain as a local excitation source, and the luminescence emitted due to SP resonance is collected by the parabolic mirror. (b) CL spectra collected at the SiO_2 part of the substrate (red), at the Si part of the substrate (black), at the Au nanodisk chain on pure Si substrate (green), and at an Au nanodisk on the silicon part of the substrate about 600 nm away from the SiO_2/Si boundary (blue), respectively. (c) SEM micrograph of the gold nanodisk chain. The color dots show the sites for CL measurements in (d). (d) CL spectra obtained by focusing an electron beam at different sites.

To investigate the propagation feature of SPs on the nanodisk chain, we measure the CL spectrum at different sites along the chain [Fig. 2(c)]. The white dashed line marks the boundary of SiO_2/Si. The colored dots denote the sites where the electron beam is focused, and the corresponding CL spectra are collected over the whole sample [Fig. 2(d)]. One may find that as the electron beam moves along the chain, the distinct peak of SiO_2 can always be observed, indicating that the SPs excited by the focused electron beam at these sites have indeed propagated on the chain. Quantitatively, we find that the normalized count of the distinctive peak of SiO_2 (425 nm) attenuates as the excitation site moves away from the SiO_2/Si boundary. This effect is due to the attenuation of the SP when it propagates on the nanodisk chain.

To explore the propagation modes of SPs on nanodisks, we fabricate a chain of Au nanodisks (diameter of 120 nm, disk separation of 10 nm) on silicon substrate, and focus an electron beam at one end of the chain to excite SPs. The CL spectrum has been collected [Fig. 3(a)]. The original data (red noisy curve) can be fitted by a blue dashed curve. Based on the analysis of Gaussian fitting multi-peaks with Origin 8 (OriginLab), three resonances peaked at 480 (green), 540 (orange), and 650 nm (purple) can be identified, which are marked by the

dashed vertical black lines in Fig. 3(a). This suggests that three resonant modes can be simultaneously excited on the chain.

Finite-difference time-domain (FDTD) simulation has been applied to explore SP resonance and propagation, where the electron beam is modeled as a series of dipoles, each with temporal phase delay according to the velocity of the electron beam [32]. The CL spectrum is simulated on the nanodisk chain with the same geometrical parameters as those in Fig. 3(a), with the electron beam source fix at the disk rim at the end of the chain. Three resonant peaks can be identified on the chain at about 480, 540, and 650 nm [Fig. 3(b)]. We can also simulate the distribution of the z component of an electric field 2 nm above the nanodisk chain, as schematically illustrated in Fig. 3(c). The distribution of the z-component of the electric field at the resonance wavelength of 480, 540, and 650 nm is shown in Fig. 3(d), which is expected to be proportional to the distribution of surface charge density [28]. At 480 nm, the field distribution on the disks designates a sequence of dipoles aligned in the x-direction [Fig. 3(d)], suggesting that there exists a sequentially connected dipole resonance on the chain. At 540 nm, the pattern on the chain turns to be a row of alternate dipoles combined with quadrupoles. The field distribution at 650 nm corresponds to the resonance of a much longer dipole, with the size of a unit cell about three times larger than that at 480 nm. Therefore, via FDTD simulation, we get a clearer picture of the resonance at 480, 540, and 650 nm, respectively.

Now we try to utilize the nanodisk chains as a beam splitter for SPs, and design an assembly of gold disks with different sizes [Fig. 4(a)]. The diameter of the largest nanodisk is 800 nm; that of the medium-sized disk is 400 nm; and that of the smallest one is 200 nm. By focusing the electron beam at the end of the largest nanodisk chain [Fig. 4(a)], we find that at least two CL peaks can be generated [Fig. 4(b)]. These two peaks correspond to two modes resonating at 540 and 730 nm, respectively. Our simulations indicate that different resonant modes correspond to different standing wave patterns on the rim of the disk, which depends on the geometrical parameters of the nanodisk. Figure 4(c) illustrates the simulated z component of electric field distribution on the nanodisk with diameters of 800, 400, and 200 nm. For the largest disks, the resonance at 540 nm possesses eight maxima (or minima) along the rim of the disk, indicating that at this wavelength an octopole resonant mode

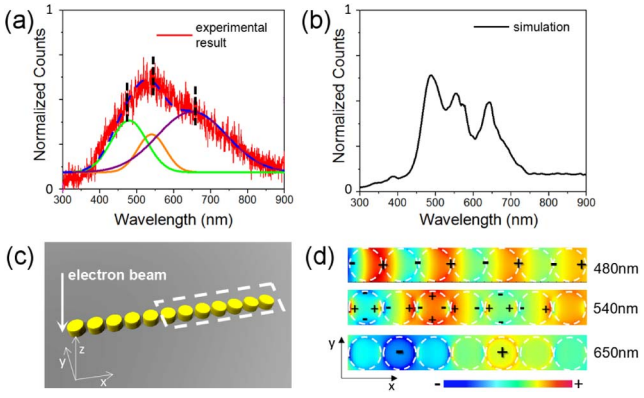

Fig. 3. (a) Spectrum measured by fixing an electron beam at one end of the chain. (b) Simulated spectrum. (c) Schematics to simulate the z components of the electric field above the chain and (d) the corresponding electric field distribution.

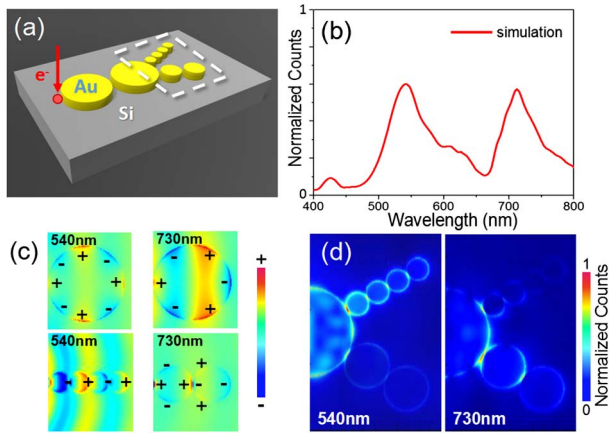

Fig. 4. (a) Designing of the beam splitter of SPs. (b) Simulated CL spectrum with the excitation site shown in (a). (c) z component of the electric field on the largest nanodisks at wavelengths of 540 and 730 nm (upper row), the medium-sized nanodisks at 730 nm (lower row, right), and the smallest nanodisks at 540 nm (lower row, left). (d) Electric field distribution showing that the SP propagates in different routes for different wavelengths.

exists on the chain. The other resonance occurs at wavelength 730 nm, where six maxima (or minima) exist on the rim of the largest disk, suggesting that this is a sextupole resonance. Similarly, for the chain made of medium-sized nanodisks, the distribution of the z component of the electric field shows a series of quadrupoles at 730 nm, in which each quadrupole has been rotated for 90° with respect to its adjacent ones. For the chain made of the smallest disks, a resonance occurs at 540 nm, where the distribution of the electric field shows a sequence of dipoles, suggesting a dipole resonant mode on the chain. FDTD simulation shows that the nanodisks with different sizes may indeed couple SPs of different wavelengths to different channels. The simulated distribution of the electric field of 2 nm above the disks is shown in Fig. 4(d), where the SPs with wavelengths of 540 nm propagate along the chain made of the smallest-sized disks [left in Fig. 4(d)], whereas SPs with wavelengths of 730 nm propagate on the chain made of medium-sized disks [right in Fig. 4(d)]. In this way, a beam splitter for SPs has been designed.

For efficient transmission of SPs of certain wavelength, the angle of the split light transmission with respect to that of the original light depends on the geometrical parameters of the disks. At the junction site (splitting site), only when the antinode on the rim of a disk with different sizes coincides, electromagnetic energy can be more efficiently propagated. This reminds us of the principle in designing the propagation circuit of SPs: the size and the angle of the side branches should be carefully selected in order to guarantee that at the junction site the antinode coincides on each branch.

Usually the field distribution simulated in Fig. 4(d) is detected by near-field scanning optical microscopy. With CL spectroscopy, however, we can sense the resonance on the structure and get the relationship between the propagation wavelength and the nano disk size. Figures 5(a) and 5(b) illustrate the CL spectra collected when the electron beam is focused at difference locations. By focusing the electron beam at site 1, two peaks at about 540 and 730 nm are observed in

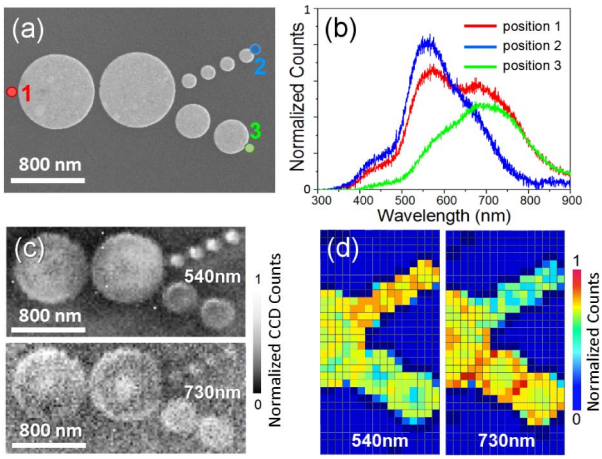

Fig. 5. (a) SEM micrograph of the splitter. (b) Spectra measured at sites 1–3 shown in (a). (c) CL spectral mapping with a pattern of maximum at two resonance wavelengths. (d) Simulation of the spectral mapping.

the CL spectrum [red curve in Fig. 5(b)]. However, by focusing the electron beam at site 2, a shorter wavelength resonant peak (blue curve) occurs. Excitation at site 3 generates a peak with a longer wavelength (green curve).

Instead of collecting a luminescence spectrum by focusing an electron beam at the specific spot, as shown in Figs. 5(a) and 5(b), we scan the structural surface point by point and collect the luminescence spectrum over the whole sample for each point excitation. Figure 5(c) shows the obtained luminescence intensity at wavelengths of 540 and 730 nm. Those sites with stronger intensity indicate that an electron beam induces stronger CL emission. At the top micrograph of Fig. 5(c), at a wavelength of 540 nm, a dark spot exists in the center of the largest disk, together with a diffused ring between the bright rim and the dark center; at 730 nm, however, a bright spot exists in the center of the largest disk, and between the bright rim and the bright center, there is a diffused dark ring. On the medium- and small-sized disks, our CL system fails to provide detailed information due to the limitation of resolution. Yet, one may still identify that the smallest nanodisk branch can be more efficiently excited at a shorter wavelength, while the medium-sized nanodisks can be more efficiently excited at longer wavelengths. The experimental observations are consistent with the FDTD simulation, as shown in Fig. 5(d).

To summarize, with CL spectroscopy, we provide here the evidence of propagation of SPs along a chain of gold nanodisks. Higher-frequency SPs transmit well on a chain with smaller gold disks, whereas lower-frequency SPs transmit more easily on a chain with larger gold disks. A beam splitter for SPs has been realized, which can be applied to selectively transmit SPs with certain frequencies to the specific directions. We expect that our observations provide the microscopic information of SP excitation and propagation on a chain of metallic nanodisks, and are insightful in designing subwavelength optical devices.

Funding. National Natural Science Foundation of China (NSFC) (11474157, 11574141, 11634005, 11674155, 61475070); Natural Science Foundation of Jiangsu Province (BK20160065); State Key Program for Basic Research from MOST of China (2012CB921502).

REFERENCES

1. H. Raether, *Surface Plasmons on Smooth and Rough Surfaces and on Gratings* (Springer-Verlag, 1988).
2. W. L. Barnes, A. Dereux, and T. W. Ebbesen, Nature**424**, 824 (2003).
3. D. R. Smith, W. J. Padilla, D. C. Vier, S. C. Nemat-Nasser, and S. Schultz, Phys. Rev. Lett.**84**, 4184 (2000).
4. R. A. Shelby, D. R. Smith, and S. Schultz, Science**292**, 77 (2001).
5. N. Fang, H. Lee, C. Sun, and X. Zhang, Science**308**, 534 (2005).
6. I. I. Smolyaninov, Y. J. Hung, and C. C. Davis, Science**315**, 1699 (2007).
7. N. Yu, P. Genevet, M. A. Kats, F. Aieta, J.-P. Tetienne, F. Capasso, and Z. Gaburro, Science**334**, 333 (2011).
8. H. Wei, Z. Wang, X. Tian, M. Käll, and H. Xu, Nat. Commun.**2**, 387 (2011).
9. Y. M. Liu and X. Zhang, Chem. Soc. Rev.**40**, 2494 (2011).
10. Z. Fang and X. Zhu, Adv. Mater.**25**, 3840 (2013).
11. P. Genevet, N. Yu, F. Aieta, J. Lin, M. A. Kats, R. Blanchard, M. O. Scully, Z. Gaburro, and F. Capasso, Appl. Phys. Lett.**100**, 013101 (2012).
12. S. C. Jiang, X. Xiong, Y. S. Hu, Y. H. Hu, G. B. Ma, R. W. Peng, C. Sun, and M. Wang, Phys. Rev. X**4**, 021026 (2014).
13. M. Quinten, A. Leitner, J. R. Krenn, and F. R. Aussenegg, Opt. Lett.**23**, 1331 (1998).
14. S. A. Maier, P. G. Kik, H. A. Atwater, S. Meltzer, E. Harel, B. E. Koel, and A. A. G. Requicha, Nat. Mater.**2**, 229 (2003).
15. S. A. Maier, M. L. Brongersma, P. G. Kik, S. Meltzer, A. A. G. Requicha, and H. A. Atwater, Adv. Mater.**13**, 1501 (2001).
16. K. L. Kelly, E. Coronado, L. L. Zhao, and G. C. Schatz, J. Phys. Chem. B**107**, 668 (2003).
17. M. D. Arnold, M. G. Blaber, M. J. Ford, and N. Harris, Opt. Express**18**, 7528 (2010).
18. Z. Wu, H. M. Li, X. Xiong, G. B. Ma, M. Wang, R. W. Peng, and N. B. Ming, Appl. Phys. Lett.**94**, 041120 (2009).
19. Y. Y. Weng, B. Zhang, S. J. Fu, M. Wang, R. W. Peng, G. B. Ma, D. J. Shu, and N. B. Ming, Phys. Rev. E**81**, 051607 (2010).
20. M. L. Brongersma, J. W. Hartman, and H. A. Atwater, Phys. Rev. B**62**, R16356 (2000).
21. C. Dahmen, B. Schmidt, and G. von Plessen, Nano Lett.**7**, 318 (2007).
22. Q. Hu, J. Z. Zhao, R. W. Peng, F. Gao, R. L. Zhang, and M. Wang, Appl. Phys. Lett.**96**, 161101 (2010).
23. B. Willingham and S. Link, Opt. Express**19**, 6450 (2011).
24. D. Li, L. Qin, X. Xiong, R. W. Peng, Q. Hu, G. B. Ma, H. S. Zhou, and M. Wang, Opt. Express**19**, 22942 (2011).
25. E. S. Barnard, T. Coenen, E. J. R. Vesseur, A. Polman, and M. L. Brongersma, Nano Lett.**11**, 4265 (2011).
26. F. F. Wen, J. Ye, N. Liu, P. Van Dorpe, P. Nordlander, and N. J. Halas, Nano Lett.**12**, 5020 (2012).
27. M. Frimmer, T. Coenen, and A. F. Koenderink, Phys. Rev. Lett.**108**, 077404 (2012).
28. K. H. Fung, A. Kumar, and N. X. Fang, Phys. Rev. B**89**, 045408 (2014).
29. T. Coenen, F. B. Arango, A. F. Koenderink, and A. Polman, Nat. Commun.**5**, 3250 (2014).
30. E. J. R. Vesseur, R. Waele, M. Kuttge, and A. Polman, Nano Lett.**7**, 2843 (2007).
31. J. B. Lassiter, H. Sobhani, M. W. Knight, W. S. Mielczarek, P. Nordlander, and N. J. Halas, Nano Lett.**12**, 1058 (2012).
32. P. Chaturvedi, K. H. Hsu, A. Kumar, K. H. Fung, J. C. Mabon, and N. X. Fang, ACS Nano**3**, 2965 (2009).